Upper Ocean O_2 trends: 1958-2015

Takamitsu Ito [1], Shoshiro Minobe [2,3], Matthew C. Long [4], and Curtis Deutsch [5]

[1]Georgia Institute of Technology, Atlanta, Georgia, USA.

[2]Department of Natural History Sciences, Graduate School of Science, Hokkaido University, Sapporo, Japan.

[3]Department of Earth and Planetary Sciences, Faculty of Science, Hokkaido University, Sapporo, Japan.

[4]Climate and Global Dynamics Laboratory, National Center for Atmospheric Research, Boulder, Colorado, USA.

[5]School of Oceanography, University of Washington, Seattle, Washington, USA.

Key Points:

- A widespread negative O_2 trend is beginning to emerge from the envelope of inter-annual variability
- The global ocean O_2 inventory is negatively correlated with the global ocean heat content
- Variability and trends in the observed upper ocean O_2 concentration are dominated by the Apparent Oxygen Utilization

Corresponding author: Taka Ito, `taka.ito@eas.gatech.edu`

Abstract

Historic observations of dissolved oxygen (O_2) in the ocean are analyzed to quantify multi-decadal trends and variability from 1958 to 2015. Additional quality control is applied and the resultant oxygen anomaly field is used to quantify upper ocean O_2 trends at global and hemispheric scales. A widespread negative O_2 trend is beginning to emerge from the envelope of interannual variability. Ocean reanalysis data is used to evaluate relationships with changes in ocean heat content (OHC) and oxygen solubility ($O_{2,sat}$). Global O_2 decline is evident after the 1980s, accompanied by an increase in global OHC. The global upper ocean O_2 inventory (0-1,000m) changed at the rate of $-243\pm124 TmolO_2$ per decade. Further, the O_2 inventory is negatively correlated with the OHC (r=-0.86; 0-1,000m) and the regression coefficient of O_2 to OHC is approximately -8.2 ± 0.66 nmol O_2 J^{-1}, on the same order of magnitude as the simulated O_2-heat relationship typically found in ocean climate models. Variability and trends in the observed upper ocean O_2 concentration are dominated by the Apparent Oxygen Utilization (AOU) component with relatively small contributions from $O_{2,sat}$. This indicates that changing ocean circulation, mixing and/or biochemical processes, rather than the direct thermally-induced solubility effects, are the primary drivers for the observed O_2 changes. The spatial patterns of the multi-decadal trend include regions of enhanced ocean deoxygenation including the subpolar North Pacific, eastern boundary upwelling systems and tropical oxygen minimum zones. Further studies are warranted to understand and attribute the global O_2 trends and their regional expressions.

1 Introduction

In this and following centuries, marine ecosystems will likely face multiple stressors as a consequence of high-CO_2 and a warming climate. The three factors—temperature increase, ocean acidification, and ocean deoxygenation—are global-scale phenomena with significant regional variations, influencing the ecosystem and biogeochemical cycles in ways not yet fully documented [*Gruber*, 2011]. Unraveling the nature and the consequences of these changes is one of the grand challenges for the ocean science community. The three factors are related to one another, that deoxygenation likely results in increased ocean acidification in subsurface waters. Such waters commonly supply nutrient to continental shelves, especially in upwelling regions. Thus, a better understanding of deoxygenation will improve our understanding of ocean acidification.

Earth System Model (ESM) simulations predict that the ocean's O_2 content is sensitive to climate warming, suggesting a significant decline of global O_2 inventory under warming scenarios out to 2100 [*Keeling et al.*, 2010]. While widespread O_2 decline in

the extratropical thermocline is a robust projection of the current generation of the ESMs, there are significant differences among models especially in the tropics [*Bopp et al.*, 2013; *Cocco et al.*, 2013]. In a warming climate, increasing seawater temperature decreases oxygen solubility, thereby reducing concentrations assuming all other factors being equal. Furthermore, increased upper ocean stratification associated with surface warming (and increased precipitation and glacier melt) can weaken ventilation, the exchange of well-oxygenated surface waters with the interior ocean. These two mechanisms reinforce one another to deplete the subsurface oxygen on the centennial timescale [*Bopp et al.*, 2002; *Plattner et al.*, 2002].

Numerous attempts have been made to detect low-frequency variability and long-term trends of subsurface O_2 using historic datasets [*Andreev and Baturina*, 2006; *Emerson et al.*, 2004; *Helm et al.*, 2011; *Johnson and Gruber*, 2007; *Ono et al.*, 2001; *Sasano et al.*, 2015; *Stendardo and Gruber*, 2012; *Stramma et al.*, 2008; *van Aken et al.*, 2011; *Whitney et al.*, 2007; *Schmidtko et al.*, 2017]. Analysis of historic datasets poses significant challenges due to sparse and irregular sampling, making the detection of long-term trends a signal-noise problem [*Long et al.*, 2016]. The global compilation by *Garcia et al.* [2005] revealed significant decadal variability of O_2, AOU and heat content in the upper 100 m for the period of 1955 through 1998. In this time period the magnitude of long-term linear trends of O_2 and AOU are relatively small compared to the decadal-scale fluctuations. *Schmidtko et al.* [2017] included additional data through recent years to calculate the O_2 trends, reporting a significant long-term trend at the rate of -257.5±185.1TmolO$_2$ (Tmol=10^{12}mol) per decade for the upper 1,200m of global oceans, equivalent of about 2±1.5% loss of the O_2 inventory for the last 50 years. In this study we build on these previous observational efforts; we examine trends in global-scale upper ocean oxygen for the period 1958 through 2015 and examine its relationship with the ocean heat content (OHC) changes.

2 Method

Additional quality control is applied to develop objectively mapped monthly climatologies of O_2 based on the World Ocean Database 2013 [WOD13; *Boyer et al.*, 2013] at standard depths specified in the dataset. We use an iterative process to construct observationally-based O_2 anomaly fields. Initially, we assemble monthly climatologies using all available data. We then construct the O_2 anomaly fields by subtracting the monthly climatologies from the observed O_2 values. Then we perform the quality control to remove questionable data points that are defined as outliers beyond three times the standard deviation of the anomalies at each point in space. When the questionable data points are removed, we

re-calculate the monthly climatologies and repeat the quality control procedure twice in order to minimize questionable data points and biases in climatologies. Anomaly data is binned annually, and the baseline for the anomalies are referenced to the 1950-2015 long-term mean. The resulting O_2 anomaly fields are then objectively mapped onto the global $1° \times 1°$ latitude/longitude grid for each standard depth. A Gaussian weight function is used for the objective mapping with the zonal and meridional length scales of 1,000 km and 500 km, respectively. The data coverage is sparse and uneven, and the sampling density is particularly low in remote regions such as the central subtropical gyres. While the relatively large radius of influence is used to reduce data gaps, it can erroneously blend information across physically separated waters, for example, between marginal seas and open oceans. Regional masks are used for the Mediterranean Sea and the Japan Sea but for the other marginal seas the data from the nearby open ocean can be blended in, which requires caution in the interpretation.

The distribution of O_2 solubility is estimated using temperature and salinity from ocean reanalysis products: the ECMWF Ocean Reanalysis (ORAS4) [*Balmaseda et al.*, 2013] and the Simple Ocean Data Assimilation (SODA version 2.2.4) [*Carton et al.*, 2000]. Rather than using raw data, we rely on the data assimilation products that are dynamically consistent and are constained by a suite of hydrographic and satellite observations. For each product, we sample the temperature and salinity at the time and location of the O_2 data points and calculate corresponding oxygen solubility ($O_{2,sat}$) [*Garcia and Gordon*, 1992]. This calculation allows us to separate O_2 variability into two components: (1) anomalies driven by changes in the solubility of O_2 and (2) anomalies driven by changes in the Apparent Oxygen Utilization ($-AOU = O_2 - O_{2,sat}$). We compute the AOU component by residual, subtracting changes that can be explained by solubility from the total O_2 anomaly. The AOU component reflects the cumulative effect of biological O2 consumption and the preformed O2 value of the source waters, thus it depends on ocean circulation, mixing and biochemical processes. Upper ocean heat content is also calculated using the ocean reanalysis products.

Three factors motivate a focus on O_2 variability in the upper ocean. First, the upper ocean O_2 has significant ecological impacts due to proximity to surface ocean habitats. Secondly, upper ocean processes are strongly affected by atmosphere-ocean interactions, thus upper ocean O_2 is likely sensitive to climate variability. Thirdly, the upper ocean is relatively well sampled, enabling more robust analysis with less uncertainty. Even so, significant uncertainty still exists due to the sparse and uneven distribution of data coverage both in time and space. The temporal data coverage is relatively poor in the earliest (1950s) and latest (2010s) part of the time series since some of the latest observations

121 have not yet been included in the database. We examine regional data coverage by count-

122 ing the number of years with observations for each $1° \times 1°$ cells of the objectively mapped

123 field (see supplementary figure S1).

124 With this sparse sampling in mind, we compile the time series of the normalized O_2

125 inventory in the upper ocean above 1,000 m depth by performing the following calcula-

126 tion,

$$I_{O2}(t) = \left(\frac{V_{obs}(t)}{V_{tot}} \right)^{-1} \int O_2'(\mathbf{x}, t) \, dV, \qquad (1)$$

127

128 where $O_2'(\mathbf{x}, t)$ is the oxygen anomaly, V_{tot} is the total volume of water and $V_{obs}(t)$ is

129 the volume of grid cells filled with O_2 data. The volume integration is based on the same

130 standard depths as the World Ocean Database.

131 The integral in Eq. (1) is performed with missing data being replaced with zeros,

132 but this produces spurious variability reflecting the year-to-year changes in sampling den-

133 sity. In order to correct for this bias, the inventory is normalized by the volumetric sam-

134 pling ratio, $(V_{obs}(t)/V_{tot})$. This correction effectively amplifies the signal when a rela-

135 tively small volume is sampled, implicitly assuming that the global mean O_2 is correctly

136 represented by the sample mean.

137 In order to examine the potential errors associated with this method of calculating

138 the global O_2 inventory with relatively sparse observations, we analyze a "large" ensem-

139 ble of simulations conducted with the Community Earth System Model-Large Ensemble

140 (CESM-LE) project [*Kay et al.*, 2015]. The CESM-LE included 35 ensemble members

141 with ocean biogeochemistry output. The model is spun up to the preindustrial conditions

142 referenced to year 1850 and a single ensemble member was integrated from 1850 to 1920.

143 Additional ensemble members are generated at 1920 by making small ($O(10^{-14})$ K) per-

144 turbations in the air temperature field and integrated for 181 years from 1920 through

145 2100, forced by historical forcing through 2005 and by the RCP8.5 forcing from 2006

146 to 2100. The quality of the O_2 simulation is discussed by *Long et al.* [2016]; briefly, the

147 model simulates a realistic distribution of O_2, but tends to have concentrations and vari-

148 ability (including trends) that are biased low. Even though the model is not perfect, many

149 realizations of the oxygen variability fields allow to evaluate the potential sampling bias in

150 the context of a single mechanistic model.

151 We calculate the sub-sampled O_2 inventories in the CESM-LE according to the ob-

152 servational sampling pattern including the increased footprint of the data through the ob-

153 jective mapping. The subsampled O_2 inventories are then adjusted according to Eq. (1).

154 We then compare these to the true O_2 inventories for each ensemble member from 1955

155 to 2015 (figure S2). About 86% of the members (30 out of 35 ensembles) estimated the

magnitude of the linear trend to be within the range of -30%+8% of the true trend in the CESM-LE simulations. There is a general tendency that the sub-sampled O_2 inventories underestimate the true global O_2 trend. In 28 out of 35 ensemble members, the linear trend (1958-2015) of sub-sampled O_2 inventories under-estimates the true trend. This indicates that there are regions outside the observational sampling pattern that have stronger trends in O_2 in the CESM-LE simulations. In general, we are encouraged that the existing observations have enough coverage to yield the correct sign of the global trend and the first-order approximation of its magnitude in the context of the CESM-LE.

3 Results

3.1 Global O_2 inventory

The normalized global O_2 inventory is plotted in figure 1a for different depth ranges. Overall the O_2 content increases slightly prior to the mid-1980s, followed by a strong decline after the mid-1980s. This pattern is consistent with the earlier study of *Garcia et al.* [2005] who focused on the upper 100 m inventory for the period of 1955-1998. For the period of 1958 to 2015, the linear trend of upper ocean O_2 inventory (0-1,000m) is -243±124TmolO_2 (Tmol=10^{12}mol) per decade, in agreement with the result of a recent independent study [*Schmidtko et al.*, 2017]. We find that a similar pattern exists throughout the upper 1,000 m of the water column and that the declining trend after the mid-1980s has persisted until recent years. Regression analysis shows that approximately 46% of the variability of the O_2 content occurs above 400 m, and 78% of the variability occurs above 700 m. Figure 1c shows the volumetric sampling ratio, $V_{obs}(t)/V_{tot}$ which is the normalization factor for the O_2 inventory (Eq. 1). The sampling ratio generally exceeds 40% between 1960 and 2010, but most recent years have significantly lower sampling ratio, in part because recent data are not yet included in the database. We expect an increased uncertainty for the most recent years due to sparser sampling; the computed O_2 inventory after 2010 may change significantly when all available data are included in the database.

Figure 1b shows the global OHC based on the ORAS4 dataset. *Balmaseda et al.* [2013] examines the data sources and their calculation of global OHC in detail. There is a slight difference in the OHC time series between the ORAS4 and the WOD13 which shows a long-term positive trend for the entire time period (see https://www.nodc.noaa. gov/OC5/3M_HEAT_CONTENT/). The time evolution global OHC is dominated by the multi-decadal warming trend with a few episodic cooling events. The cooling episodes matches with the period of volcanic eruptions (El Chichon in 1982 and Mt Pinatubo in 1991) and the period following the 1997-1998 El-Nino event. The normalized O_2 inven-

190 tory is compared to the OHC time series (Figure 1d). The two time series are significantly

191 correlated according to a *t*-test (r=−0.86, 95% CI for 0-1,000 m OHC and O_2).

192   The regression reveals the relationship between the changes in the OHC and the O_2

193 inventory. Centennial-scale global warming simulations using ESMs predict that the O_2-

194 heat ratio to be between −5.9 and −6.7 nmol O_2 J^{-1} [*Keeling et al.*, 2010]. For the nor-

195 malized O_2 inventory and the OHC above the 1,000 m depth, the regression coefficient is

196 −8.2±0.66 nmol O_2 J^{-1}. The overall agreement in the O_2-heat ratio is remarkable given

197 the uncertainties in the inventory calculation and the potential model errors. A close ex-

198 amination of Figure 1d reveals that the slope of O_2-heat relationship is flatter at shallower

199 depths. The O_2-heat ratio is not uniform spatially; the O_2 inventory appears to be less sen-

200 sitive to the changes in OHC in the shallower waters, and the ratio increases with depth

201 (supplementary information, Table S1). Above the 100 m depth, the regression coefficient

202 is −1.96±1.27 nmol O_2 J^{-1}, consistent with the expected relationship based on the tem-

203 perature dependence of solubility [*Keeling and Garcia*, 2002]. While the linkages between

204 the O_2 content and OHC is not fully understood, the observation suggests that the O_2 in-

205 ventory in/below the thermocline is significantly more sensitive to the OHC. This may

206 indicate the crucial role played by the ventilation and the circulation changes of the deeper

207 water masses which may reflect the freshening and warming of the water column. This re-

208 sult is consistent with the recent study by *Schmidtko et al.* [2017] that the O_2 trends above

209 the main thermocline are primarily controlled by the temperature dependence of O_2 solu-

210 bility, and the AOU component becomes dominant in the deeper waters.

3.2 Global and hemispheric trends in O_2, $O_{2,sat}$ and AOU

212   To further investigate the upper ocean O_2 changes, we examine the global and hemi-

213 spheric area-weighted mean O_2 time series for three depth levels at 100 m, 200 m and

214 400 m. We include results from the 200 m depth as Figure 2 in the main text; data from

215 the 100 m and 400 m depths are also shown in the supplementary document (Figure S3

216 and S4). Our calculation of the linear trend and its statistical significance is based on the

217 method of adjusted standard error and adjusted degrees of freedom following *Santer et al.*

218 [2000], wherein a *t*-test is used to evaluate whether or not the observed linear trend is sig-

219 nificantly different from zero. Figure 2ace shows the global and hemispheric time series of

220 O_2, O_2^{sat} and the negative of AOU at the depth of 200 m. As described above, we com-

221 pute the negative of AOU as a residual, subtracting the solubility component from the

222 total O_2 anomaly, thus the AOU component captures the O_2 variability not explained by

223 the solubility changes. There are two estimates of O_2^{sat} from the ORAS4 and SODA2.2.4

224 products which have different temperature/salinity distributions. The two reanalyses agree

225 in the overall magnitude of the $O_{2,sat}$ variability which is much smaller than that of O_2;

226 therefore, regardless of the reanalysis product, the AOU component dominates the O_2 vari-

227 ability and so we plot AOU based on ORAS4 only.

228 The two hemispheres both exhibit multi-decadal O_2 decline but their temporal vari-

229 abilities are different. It is important to note that the data density of the southern hemi-

230 sphere is significantly lower than the northern hemisphere, thus it is more likely influenced

231 by the sampling biases. With this caveat in mind, the global and hemispheric O_2 time

232 series show significant decline after 1980s, which is also evident at 100 m and 400 m

233 depths (see Figures S3 and S4). At 100 m depth, there is a decadal O_2 increase from the

234 1960s to 1980s for the global and northern hemispheric data as previously identified [*Gar-*

235 *cia et al.*, 2005]. Previous investigations of regional O_2 changes have also shown strong

236 O_2 decline in the Pacific basin after 1980s [*Deutsch et al.*, 2011; *Czeschel et al.*, 2012;

237 *Stramma et al.*, 2012; *Ito and Deutsch*, 2013], which may be related to the reduced ventila-

238 tion in the Sea of Okhotsk [*Ohshima et al.*, 2014; *Nakanowatari et al.*, 2007].

239 Figures 2bdf show the global and hemispheric linear trends of O_2 represented as a

240 matrix of trends with varying starting and ending years. The color shading indicates the

241 magnitude of the linear trend and the hatched regions indicate whether the trend is signif-

242 icantly differ from zero (positive or negative) with 95% confidence interval [*Santer et al.*,

243 2000]. The linear trends are sensitive to the time period of analysis due to the superpo-

244 sition of interannual variability with the multi-decadal trends. Overall the trend matrix is

245 predominantly negative, and the decreasing trends becomes statistically significant with the

246 ending year of 2005 and later. The earlier analysis [*Garcia et al.*, 2005] indeed detected

247 the beginning of post-1980s O_2 decline, despite the relatively narrow time window (1955-

248 1998). Our analysis shows that the negative trend continued to develop during 2000s.

3.3 Spatial pattern of the O_2 trend

250 Figure 3 shows the maps of the multi-decadal trend over three different depth ranges.

251 There are several regions of intense O_2 decline as noted by earlier investigations such

252 as western subpolar North Pacific [*Ono et al.*, 2001], the Gulf of Alaska [*Whitney et al.*,

253 2007], equatorial Atlantic and eastern equatorial Pacific [*Stramma et al.*, 2008; *Stramma*

254 *et al.*, 2012]. The subpolar North Pacific (SPNP) is a relatively well sampled region and

255 exhibits a significant negative trend at all depths as shown by earlier studies [*Ono et al.*,

256 2001; *Whitney et al.*, 2007]. There are also several regions of O_2 increase such as in the

257 western subtropical North Pacific and eastern subpolar North Atlantic as noticed by previ-

258 ous studies [*Helm et al.*, 2011; *Sasano et al.*, 2015].

259   Many parts of the global oceans are under-sampled, and the apparent lack of trend

260 may be an artifact of sparse observations in some regions. The open oceans in the extra-

261 tropical southern hemisphere are poorly sampled in general (Figure S1), and it is possible

262 that the relatively weak trend in the southern hemisphere (Figure 3) may be due to the

263 sparse sampling. In contrast, the Labrador Sea is a relatively well sampled region but the

264 observations do not show a significant trend there. Convective mixing and hydrographic

265 properties of the Labrador Sea are known to exhibit significant interannual and decadal

266 variability, but no significant long-term trend has been observed to date [*Yashayaev*, 2007;

267 *van Aken et al.*, 2011]. Thus, a long-term trend of O_2 is not expected in this region and

268 our result is consistent with these earlier studies.

269   Finally, we attempt to speculate the potential causes of the observed O_2 changes.

270 Solubility changes only play a secondary role below the thermocline, given the relatively

271 low variability in the $O_{2,sat}$ component; thus, the O_2 variability is predominantly con-

272 trolled by AOU changes for the global averages. The changes in AOU can come from

273 many factors; the preformed O_2 value at the location of water mass formation, the rates

274 of biochemical O_2 consumption, the rates of subduction, eddy mixing, and shifts in wa-

275 ter mass boundaries. The circulation and eddy stirring can modulate the physical sup-

276 ply of O_2 affecting the regional patterns of O_2 changes [*Stramma et al.*, 2010; *Czeschel*

277 *et al.*, 2011; *Llanillo et al.*, 2013; *Brandt et al.*, 2015]. Figure 3 shows the contrast be-

278 tween the subpolar and subtropical North Pacific where the O_2 strongly decreases in the

279 subpolar region and it slightly increases in the subtropics. The increase of subtropical O_2

280 is consistent with the expansion of winter-time isopycnal outcrop where O_2-rich surface

281 waters subduct into the thermocline [*Kwon et al.*, 2016]. In the subpolar region the ther-

282 mocline waters are not directly ventilated from the open ocean but the source waters are

283 formed in the marginal seas of the northwestern North Pacific and are strongly influenced

284 by the mixing at the Oyashio front and Kuroshio extension regions [*Talley*, 1993]. The

285 O_2 decline in the SPNP may reflect the changes in the source regions such as the Sea of

286 Okhotsk or the mixing processes. In the tropical oxygen minimum zones, the ocean cli-

287 mate and circulation variability can shift water masses and alter the rate of nutrient supply

288 to the surface euphotic layer and drive decadal O_2 variability [*Deutsch et al.*, 2011].

289 **4 Discussion**

290   The World Ocean Database 2013 [*Boyer et al.*, 2013] is used to calculate the global

291 O_2 inventory and hemispheric O_2 trends for the period of 1958 to 2015. The distribu-

292 tion of observations is relatively sparse, omitting large regions of the oceans; however, we

293 demonstrate that this distribution is sufficient to robustly estimate global O_2 trends in the

context of an Earth system model simulation. An earlier study [*Garcia et al.*, 2005] with a shorter record period (1955–1998) found little evidence of a long term trend, but our analysis shows that the addition of 17 years of observations has revealed a widespread negative O_2 trend beginning to emerge from the envelope of interannual variability. In conjunction with the O_2 trend, the O_2 solubility and the ocean heat content is examined using temperature and salinity data from ORAS4 [*Balmaseda et al.*, 2013] and SODA2.2.4 [*Carton et al.*, 2000]. Consistent with previous studies, observed O_2 variability is dominated by AOU changes regardless of the dataset used for the temperature and salinity. This indicates that O_2 changes are predominantly driven by changing ocean ventilation and/or biological O_2 consumption. Furthermore, the O_2 inventory is significantly correlated with changes in ocean heat content, particularly for thermocline and deep waters, indicating linkages between the ocean heat uptake and the global AOU increase.

The mechanisms behind the AOU change are not fully understood. In a warming ocean, the surface heating , glacier melt and increased precipitation at high latitudes can increase the ocean stratification, leading to the weakened mixing of O_2-rich surface waters into the thermocline. Earth System Models indeed predict a long term O_2 decline (and increase of AOU as well as ventilation age) on the centennial timescales [*Cocco et al.*, 2013; *Bopp et al.*, 2013; *Long et al.*, 2016]. This mechanism could be at play for the last several decades of O_2 data analyzed here.

The observed O_2 decline is not uniform in space. Relatively strong and widespread O_2 decline is found in the subpolar North Pacific and in the tropics; whereas the subtropical North Pacific shows a moderate O_2 increase. This pattern has been identified by earlier studies in association with increasing upper ocean stratification [e.g. *Ono et al.*, 2001; *Emerson et al.*, 2004; *Stramma et al.*, 2012], and *Ito et al.* [2016] showed that this pattern may have been caused by the combined effects of natural climate variability and the deposition of polluted dust over the North Pacific Ocean. A recent study [*Long et al.*, 2016] showed that the spatial patterns of O_2 change are similar between the centennial, anthropogenically-forced trend and interannual variability. On this basis, it is possible that the strong O_2 change in the subpolar North Pacific can be caused by either natural climate variability, warming induced long-term change, or some combination of the two.

While climate trends and variability are clearly important drivers of observed O_2 changes, a wider range of processes can contribute to the O_2 changes. For example, *Riebesell et al.* [2007] showed that the C:N utilization ratio of organic matter production in a mesocosm experiment increased under high CO_2 conditions. If this relationship scales globally, the effect could yield larger C:N ratios in sinking organic matter, thereby driving subsurface oxygen declines under high CO_2 conditions (presuming C:O_2 stoichiometry

of aerobic respiration remains the same). This effect was included in a modeling study [*Oschlies et al.*, 2008], which showed a 50% increase in the global volume of suboxic ($O_2 < 5\mu M$) waters by 2100 due to increasing C:N ratios in sinking organic matter relative to experiments omitting this effect. In addition to changing C:N utilization ratios, increased exogenous nutrient inputs could drive increased carbon export and oxygen utilization in the interior. *Krishnamurthy et al.* [2010], for instance, simulated anthropogenic enhancements of aerosol nutrient deposition in an Earth system model. Their simulation showed an increase in the biological productivity in the Pacific basin stimulated by the additional nutrient input from aerosols. Interestingly, the simulated O_2 change in the North Pacific was only moderate in this particular model, and the authors commented that the circulation variability may be more important in driving O_2 variability in this region.

While these perturbations to nutrient cycling could alter the O_2 trends over time, our result reveals a tight relationship between O_2 inventories and OHC. The spatial structure and magnitude of this relationship are consistent with expectations derived from mechanistic models forced under climate warming scenarios. This study owes its existence to the international collaboration through the World Ocean Database Project, and it is crucial to maintain and support the collection and submission of the data. Unfortunately, the spatiotemporal distribution of O_2 observations remains too sparse for definitive conclusions and attribution. However, taken together, the evidence is consistent with anthropogenic warming acting as the primary driver of long-term trends in ocean O_2. The trends we document are suggestive of the effects of warming beginning to supersede natural variability and emerge as a recognizable signal. This merits additional scrutiny over the coming years; if it is the warming signal, we should expect to see continued widespread declines in oceanic O_2. The impacts of ocean deoxygenation on ocean ecosystems may be profound. In this light, it is critical to develop improved understanding of the mechanisms driving trends and variability in the oceanic O_2. The scientific community should work to ensure adequate observing capabilities are maintained; we have an obligation to document and communicate these impacts of warming, such that society can make informed decisions and understand costs/benefits trade-offs for mitigation.

paper. Data analysis products used to generate the figures and tables are available from the corresponding author upon request.

References

Andreev, A. G., and V. I. Baturina (2006), Impacts of tides and atmospheric forcing variability on dissolved oxygen in the subarctic North Pacific, *J. Geophys. Res.*, *111*(C7), C07S10, doi:10.1029/2005JC003103.

Balmaseda, M. A., K. Mogensen, and A. T. Weaver (2013), Evaluation of the ECMWF ocean reanalysis system ORAS4, *Q. J. R. Meteorol. Soc.*, *139*(674), 1132–1161, doi:10. 1002/qj.2063.

Bopp, L., C. Le Quéré, M. Heimann, A. C. Manning, and P. Monfray (2002), Climate-induced oceanic oxygen fluxes: Implications for the contemporary carbon budget, *Global Biogeochem. Cycles*, *16*, 1022, doi:10.1029/2001GB001445.

Bopp, L., L. Resplandy, J. C. Orr, S. C. Doney, J. P. Dunne, M. Gehlen, P. Halloran, C. Heinze, T. Ilyina, R. Séférian, J. Tjiputra, and M. Vichi (2013), Multiple stressors of ocean ecosystems in the 21st century: projections with CMIP5 models, *Biogeosci.*, *10*, 6225–6245, doi:10.5194/bg-10-6225-2013.

Boyer, T., J. I. Antonov, O. K. Baranova, C. Coleman, H. E. Garcia, A. Grodsky, D. R. Johnson, R. A. Locarnini, A. V. Mishonov, T. O'Brien, C. Paver, J. Reagan, D. Seidov, I. V. Smolyar, and M. M. Zweng (2013), World ocean database 2013, in *NOAA Atlas NESDIS*, vol. 72, edited by S. Levitus and A. Mishonov, p. 209 pp, doi:10.7289/ V5NZ85MT.

Brandt, P., H. W. Bange, D. Banyte, M. Dengler, S.-H. Didwischus, T. Fischer, R. J. Greatbatch, J. Hahn, T. Kanzow, J. Karstensen, A. Körtzinger, G. Krahmann, S. Schmidtko, L. Stramma, T. Tanhua, and M. Visbeck (2015), On the role of circulation and mixing in the ventilation of oxygen minimum zones with a focus on the eastern tropical north atlantic, *Biogeosci.*, *12*(2), 489–512, doi:10.5194/bg-12-489-2015.

Bretherton, C. S., M. Widmann, V. P. Dymnikov, J. M. Wallace, and I. BladÃľ (1999), The effective number of spatial degrees of freedom of a time-varying field, *Journal of Climate*, *12*(7), 1990–2009, doi:10.1175/1520-0442(1999)012<1990:TENOSD>2.0.CO; 2.

Carton, J. A., G. Chepurin, X. Cao, and B. Giese (2000), A Simple Ocean Data Assimilation Analysis of the Global Upper Ocean 1950–95. Part I: Methodology, *J. Phys. Oceanogr.*, *30*(2), 294–309, doi:10.1175/1520-0485(2000)030<0294:ASODAA>2.0.CO; 2.

Cocco, V., F. Joos, M. Steinacher, T. L. Frölicher, L. Bopp, J. Dunne, M. Gehlen, C. Heinze, J. Orr, A. Oschlies, B. Schneider, J. Segschneider, and J. Tjiputra (2013), Oxygen and indicators of stress for marine life in multi-model global warming projections, *Biogeosciences*, *10*, 1849–1868, doi:10.5194/bg-10-1849-2013.

Czeschel, R., L. Stramma, F. U. Schwarzkopf, B. S. Giese, A. Funk, and J. Karstensen (2011), Middepth circulation of the eastern tropical south pacific and its link to the oxygen minimum zone, *J. Geophys. Res.*, *116*(C1), C01015, doi:10.1029/2010JC006565.

Czeschel, R., L. Stramma, and G. C. Johnson (2012), Oxygen decreases and variability in the eastern equatorial pacific, *Journal of Geophysical Research: Oceans*, *117*(C11), n/a–n/a, doi:10.1029/2012JC008043, c11019.

Deutsch, C., H. Brix, T. Ito, H. Frenzel, and L. Thompson (2011), Climate-forced variability of ocean hypoxia, *Science*, *333*(6040), 336–339, doi:10.1126/science.1202422.

Emerson, S., Y. Watanabe, T. Ono, and S. Mecking (2004), Temporal Trends in Apparent Oxygen Utilization in the Upper Pycnocline of the North Pacific: 1980–2000, *J. Oceanogr.*, *60*(1), 139–147, doi:10.1023/B:JOCE.0000038323.62130.a0.

Garcia, H. E., and L. I. Gordon (1992), Oxygen solubility in seawater: Better fitting equations, *Limnology and Oceanography*, *37*(6), 1307–1312, doi:10.4319/lo.1992.37.6.1307.

Garcia, H. E., T. P. Boyer, S. Levitus, R. A. Locarnini, and J. Antonov (2005), On the variability of dissolved oxygen and apparent oxygen utilization content for the upper world ocean: 1955 to 1998, *Geophy. Res. Lett.*, *32*, L09604, doi:10.1029/2004GL022286.

Gruber, N. (2011), Warming up, turning sour, losing breath: ocean biogeochemistry under global change, *Philos. Trans. Roy. Soc.*, *369*, 1980–1996, doi:10.1098/rsta.2011.0003.

Helm, K. P., N. L. Bindoff, and J. A. Church (2011), Observed decreases in oxygen content of the global ocean, *Geophy. Res. Lett.*, *38*, L23602, doi:10.1029/2011GL049513.

Ito, T., and C. Deutsch (2013), Variability of the oxygen minimum zone in the tropical north pacific during the late twentieth century, *Global Biogeochemical Cycles*, *27*(4), 1119–1128, doi:10.1002/2013GB004567.

Ito, T., A. Nenes, M. S. Johnson, N. Meskhidze, and C. Deutsch (2016), Acceleration of oxygen decline in the tropical pacific over the past decades by aerosol pollutants, *Nature Geosci*, *9*(6), 443–447, doi:10.1038/ngeo2717http://www.nature.com/ngeo/journal/v9/n6/abs/ngeo2717.html#supplementary-information.

Johnson, G. C., and N. Gruber (2007), Decadal water mass variations along 20°W in the Northeastern Atlantic Ocean, *Prog. Oceanogr.*, *73*, 277–295, doi:10.1016/j.pocean.2006.03.022.

Kay, J. E., C. Deser, A. Phillips, A. Mai, C. Hannay, G. Strand, J. M. Arblaster, S. C. Bates, G. Danabasoglu, J. Edwards, M. Holland, P. Kushner, J. F. Lamarque, D. Lawrence, K. Lindsay, A. Middleton, E. Munoz, R. Neale, K. Oleson, L. Polvani, and M. Vertenstein (2015), The community earth system model (cesm) large ensemble project a community resource for studying climate change in the presence of internal climate variability, *Bull. Amer. Meteor. Soc.*, *96*(8), 1333–1349, doi:10.1175/bams-d-13-00255.1.

Keeling, R. F., and H. E. Garcia (2002), The change in oceanic O_2 inventory associated with recent global warming, *Proc. Natl. Acad. Sci. U.S.A.*, *99*(12), 7848–7853, doi:10.1073/pnas.122154899.

Keeling, R. F., A. Körtzinger, and N. Gruber (2010), Ocean Deoxygenation in a Warming World, *Ann. Rev. of Mar. Sci.*, *2*, 199–229, doi:10.1146/annurev.marine.010908.163855.

Krishnamurthy, A., J. K. Moore, N. Mahowald, C. Luo, and C. S. Zender (2010), Impacts of atmospheric nutrient inputs on marine biogeochemistry, *J. Geophys. Res.*, *115*(G1), doi:10.1029/2009JG001115.

Kwon, E. Y., C. Deutsch, S.-P. Xie, S. Schmidtko, and Y.-K. Cho (2016), The north pacific oxygen uptake rates over the past half century, *J. Clim.*, *29*(1), 61–76, doi:10.1175/JCLI-D-14-00157.1.

Llanillo, P. J., J. Karstensen, J. L. Pelegrí, and L. Stramma (2013), Physical and biogeochemical forcing of oxygen and nitrate changes during el nino/el viejo and la nina/la vieja upper-ocean phases in the tropical eastern south pacific along 86w, *Biogeosci.*, *10*(10), 6339–6355, doi:10.5194/bg-10-6339-2013.

Long, M. C., C. A. Deutsch, and T. Ito (2016), Finding forced trends in oceanic oxygen, *Global Biogeochem. Cycles*, *30*, doi:10.1002/2015GB005310.

Nakanowatari, T., K. I. Ohshima, and M. Wakatsuchi (2007), Warming and oxygen decrease of intermediate water in the northwestern north pacific, originating from the sea of okhotsk, 1955–2004, *Geophysical Research Letters*, *34*(4), n/a–n/a, doi:10.1029/2006GL028243, l04602.

Ohshima, K. I., T. Nakanowatari, S. Riser, Y. Volkov, and M. Wakatsuchi (2014), Freshening and dense shelf water reduction in the okhotsk sea linked with sea ice decline, *Progress in Oceanography*, *126*, 71 – 79, doi:http://dx.doi.org/10.1016/j.pocean.2014.04.020, biogeochemical and physical processes in the Sea of Okhotsk and the linkages to the Pacific Ocean.

Ono, T., T. Midorikawa, Y. W. Watanabe, K. Tadokoro, and T. Saino (2001), Temporal increases of phosphate and apparent oxygen utilization in the subsurface waters of western subarctic Pacific from 1968 to 1998, *Geophy. Res. Lett.*, *28*(17), 3285–3288, doi:10.1029/2001GL012948.

Oschlies, A., K. G. Schulz, U. Riebesell, and A. Schmittner (2008), Simulated 21st century's increase in oceanic suboxia by co2-enhanced biotic carbon export, *Global Biogeochemical Cycles*, *22*(4), n/a–n/a, doi:10.1029/2007GB003147, gB4008.

Plattner, G.-K., F. Joos, and T. F. Stocker (2002), Revision of the global carbon budget due to changing air-sea oxygen fluxes, *Global Biogeochem. Cycles*, *16*, 1096, doi:10.1029/2001GB001746.

Riebesell, U., K. G. Schulz, R. G. J. Bellerby, M. Botros, P. Fritsche, M. Meyerhofer, C. Neill, G. Nondal, A. Oschlies, J. Wohlers, and E. Zollner (2007), Enhanced biological carbon consumption in a high co2 ocean, *Nature*, *450*(7169), 545–U10, doi:10.1038/nature06267.

Santer, B. D., T. M. L. Wigley, J. S. Boyle, D. J. Gaffen, J. J. Hnilo, D. Nychka, D. E. Parker, and K. E. Taylor (2000), Statistical significance of trends and trend differences in layer-average atmospheric temperature time series, *J. Geophys. Res.*, *105*(D6), 7337–7356, doi:10.1029/1999JD901105.

Sasano, D., Y. Takatani, N. Kosugi, T. Nakano, T. Midorikawa, and M. Ishii (2015), Multidecadal trends of oxygen and their controlling factors in the western North Pacific, *Global Biogeochem. Cycles*, *29*, 935–956, doi:10.1002/2014GB005065.

Schmidtko, S., L. Stramma, and M. Visbeck (2017), Decline in global oceanic oxygen content during the past five decades, *Nature*, *542*(7641), 335–339, doi:10.1038/nature21399.

Stendardo, I., and N. Gruber (2012), Oxygen trends over five decades in the North Atlantic, *J. Geophys. Res.*, *117*, C11004, doi:10.1029/2012JC007909.

Stramma, L., G. C. Johnson, J. Sprintall, and V. Mohrholz (2008), Expanding Oxygen-Minimum Zones in the Tropical Oceans, *Science*, *320*, 655–658, doi:10.1126/science.1153847.

Stramma, L., G. C. Johnson, E. Firing, and S. Schmidtko (2010), Eastern pacific oxygen minimum zones: Supply paths and multidecadal changes, *J. Geophys. Res.*, *115*(C9), C09011, doi:10.1029/2009JC005976.

Stramma, L., A. Oschlies, and S. Schmidtko (2012), Mismatch between observed and modeled trends in dissolved upper-ocean oxygen over the last 50 yr, *Biogeosciences*, *9*(10), 4045–4057, doi:10.5194/bg-9-4045-2012.

Talley, L. D. (1993), Distribution and formation of north pacific intermediate water, *Journal of Physical Oceanography*, *23*(3), 517–537, doi:10.1175/1520-0485(1993)023<0517:DAFONP>2.0.CO;2.

van Aken, H. M., M. Femke de Jong, and I. Yashayaev (2011), Decadal and multi-decadal variability of Labrador Sea Water in the north-western North Atlantic Ocean derived

508   from tracer distributions: Heat budget, ventilation, and advection, *Deep Sea Res.*, *58*,

509   505–523, doi:10.1016/j.dsr.2011.02.008.

510 Whitney, F. A., H. J. Freeland, and M. Robert (2007), Persistently declining oxygen levels

511   in the interior waters of the eastern subarctic Pacific, *Prog. Oceanogr.*, *75*, 179–199,

512   doi:10.1016/j.pocean.2007.08.007.

513 Yashayaev, I. (2007), Hydrographic changes in the labrador sea, 1960-2005 (vol 73,

514   pg242, 2007), *Progress in Oceanography*, *75*(4), 857–859, doi:10.1016/j.pocean.2007.

515   09.001.
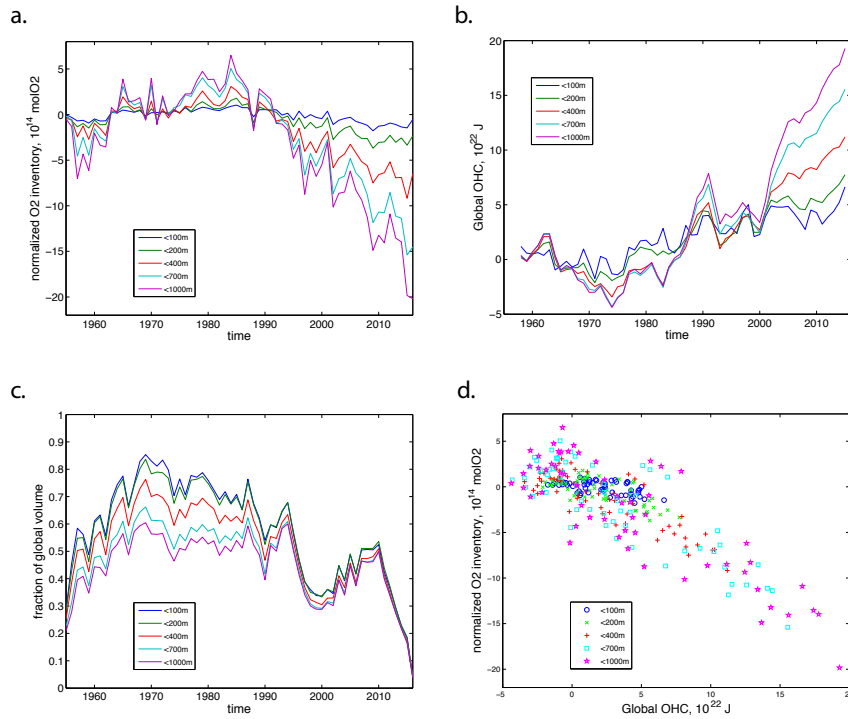
Figure 1. (a) Normalized O_2 inventory above the depths of 100m (blue), 200m (green), 400m (red), 700m (teal) and 1,000m (purple). (b) Global OHC based on the ORAS4 dataset. The color coding is the same as (a) indicating the vertical range of integration. (c) Volumetric sampling density measured as the fraction of grid cells filled with data. (d) The scatter diagram of the normalized O_2 inventory versus OHC. The significance testing of the correlation is performed according to the definition of the effective sample size according to *Bretherton et al.* [1999].
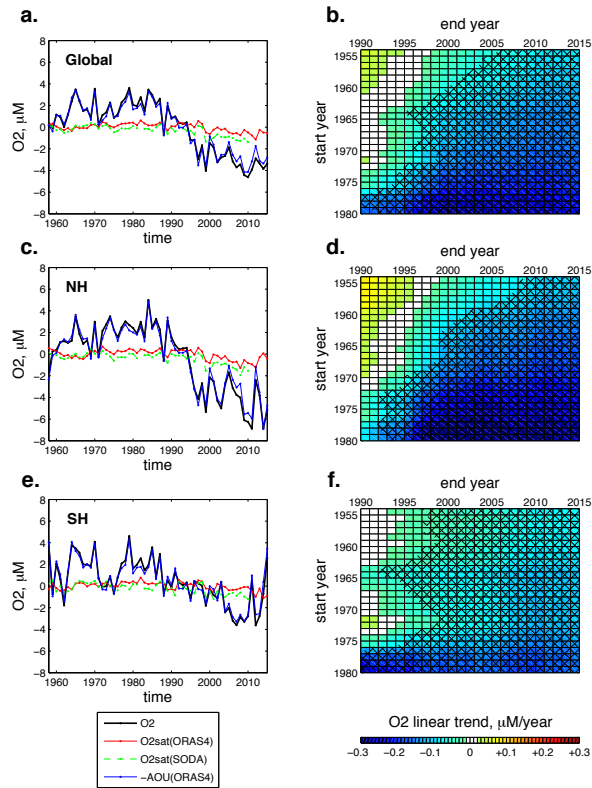
Figure 2. (a) Global O_2 time series at the depth of 200m. Data points are weighted by the cosine of latitude. Black is O_2, Red and Green are O_2 saturation based on ORAS4 and SODA2.2.4 respectively. Blue is (-1) x AOU. (b) Trend matrix is formed by taking linear trend of O_2 with different starting and ending years. Color shading shows the magnitude of the trend. Hatching is applied for positive/negative definite trends with 95% CI using the method of adjusted standard error and adjusted degree of freedom following Santer et al. [2000]. (c,d) the same as (a,b) but for the northern hemispheric data points only. (e,f) the same as (a,b) but for the southern hemispheric data points only.

a. 100m

b. 400m

c. 700m

1958-2015 O2 trend, μMyr^{-1}

-0.5   -0.3   -0.1   +0.1   +0.3   +0.5
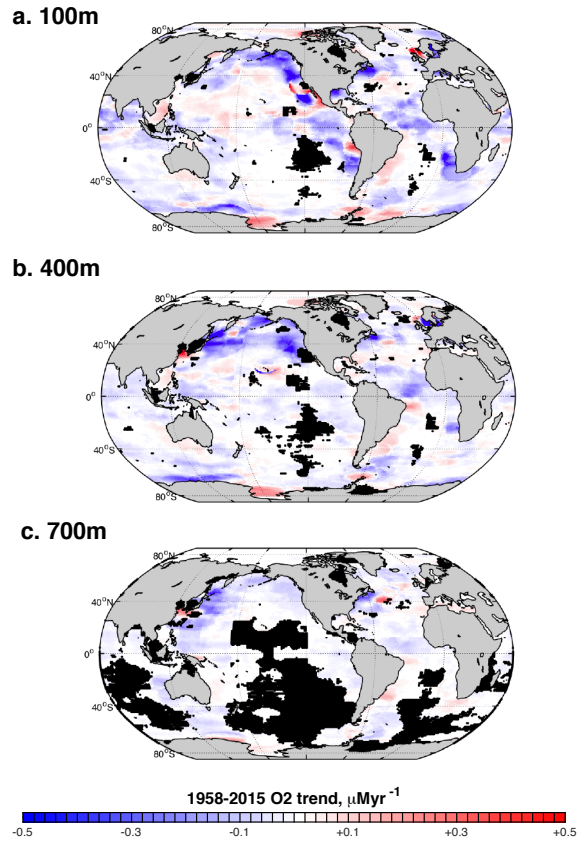
Figure 3. (a) Global map of the linear trend of O2 time series at the depth of 100m. We plot the linear trend for the grid cells where the effective sample size (N_{eff}) is greater than 20. (b) same as (a) but at the depth of 400m. (c) same as (a) but at the depth of 700m. We indicate the regions where there are insufficient data ($N_{eff} < 20$) by black dots.